TECHNICAL MEMORANDUM

TRANSONIC STATIC AND DYNAMIC LONGITUDINAL STABILITY CHARACTERISTICS OF A LOW-FINENESS-RATIO, BLUNTED-CYLINDER REENTRY BODY HAVING A CONVERGING-CONE AFTERBODY

By Ernest R. Hillje and Albin O. Pearson

Langley Research Center
Langley Station, Hampton, Va.

NATIONAL AERONAUTICS AND SPACE ADMINISTRATION
WASHINGTON
May 1962

reasonable limitation of the angle of attack. (See ref. 1.) The damping and stability characteristics of this type of body are difficult to estimate, especially at transonic speeds where flows are often unpredictable.

In order to provide information of interest in this uncertain region for a proposed reconnaissance satellite that may be required to reenter the atmosphere of the earth, transonic wind-tunnel tests were made of a scale model. The results of these tests are presented herein. In addition to the dynamic longitudinal stability characteristics, static stability characteristics are presented. The model was a low-fineness-ratio, blunted-cylinder reentry body having a converging truncated-cone afterbody. The angle-of-attack range was -3° to 18.3° for the static tests and 0° to 14° for the dynamic tests. For the dynamic tests, the model was rigidly forced to perform a sinusoidal pitching motion of 2° amplitude at reduced frequencies from 0.018 to 0.058. The Mach number range was from 0.60 to 1.20 and the Reynolds number for the tests, based on model diameter, was varied from 2.04×10^6 to 4.00×10^6. Tests were made for several types of surface conditions.

SYMBOLS

The data presented are referred to the body-axis system with the origin located at the oscillation center which was coincident with the proposed center-of-gravity position of the full-scale body. (See figs. 1 and 2.)

A	maximum cross-sectional area of model, 0.328 sq ft
d	maximum diameter of model, 0.646 ft
M	free-stream Mach number
p_t	stagnation pressure, atm
q	pitching angular velocity, radians/sec
R	Reynolds number based on d
V	free-stream velocity, ft/sec
α	angle of attack, deg or radians
ρ	free-stream mass density of air, $\frac{\text{lb-sec}^2}{\text{ft}^4}$

NATIONAL AERONAUTICS AND SPACE ADMINISTRATION

TECHNICAL MEMORANDUM X-672

TRANSONIC STATIC AND DYNAMIC LONGITUDINAL STABILITY CHARACTERISTICS OF A LOW-FINENESS-RATIO, BLUNTED-CYLINDER REENTRY BODY HAVING A CONVERGING-CONE AFTERBODY*

By Ernest R. Hillje and Albin O. Pearson

SUMMARY

The static and dynamic longitudinal stability parameters for a low-fineness-ratio, blunted-cylinder reentry body having a converging truncated-cone afterbody have been measured in the Langley 8-foot transonic pressure tunnel. Static data were taken at angles of attack from -3° to 18.3° and dynamic data at angles of attack from 0° to 14°. The dynamic tests were made with an oscillation amplitude of 2° and at reduced frequencies from 0.018 to 0.058. Reynolds number was varied from 2.04×10^6 to 4.00×10^6, and the test Mach number range extended from 0.60 to 1.20.

Results show that, in general, the body possesses static longitudinal stability throughout the ranges of the present investigation with small areas of neutral stability. The damping-in-pitch parameter varied erratically from values of approximately 3 to -2 and was affected by Mach number, angle of attack, reduced frequency, surface condition, and Reynolds number. The oscillatory longitudinal stability parameter showed good agreement with the static pitching-moment coefficients and, in general, showed stability throughout with small areas of neutral stability near an angle of attack of 4°, and except for being relatively insensitive to reduced frequency, was also dependent on the aforementioned factors.

Author

INTRODUCTION

Blunt, nonlifting reentry bodies of low fineness ratio require a certain amount of aerodynamic damping and stability as the bodies decelerate through the transonic and subsonic speed regions to insure a

*Title, Unclassified.

ω angular velocity, 2π (Frequency of oscillation), radians/sec

$\frac{\omega d}{V}$ reduced frequency parameter

C_A axial-force coefficient,
$$\frac{\text{Axial force (uncorrected for base pressure)}}{\frac{\rho}{2}V^2A}$$

C_m pitching-moment coefficient, $\dfrac{\text{Pitching moment}}{\frac{\rho}{2}V^2Ad}$

C_N normal-force coefficient, $\dfrac{\text{Normal force}}{\frac{\rho}{2}V^2A}$

$C_{p,b}$ base-pressure coefficient,
$$\frac{\text{Base pressure - Free-stream static pressure}}{\frac{\rho}{2}V^2}$$

$C_{p,c}$ model balance chamber-pressure coefficient,
$$\frac{\text{Model-balance chamber pressure - Free-stream static pressure}}{\frac{\rho}{2}V^2}$$

$C_{m_\alpha} = \dfrac{\partial C_m}{\partial \alpha}$, per radian

$C_{m_{\dot\alpha}} = \dfrac{\partial C_m}{\partial\left(\frac{\dot\alpha d}{V}\right)}$, per radian

$C_{m_q} = \dfrac{\partial C_m}{\partial\left(\frac{qd}{V}\right)}$, per radian

$C_{m_{\dot q}} = \dfrac{\partial C_m}{\partial\left(\frac{\dot q d^2}{V^2}\right)}$, per radian

$C_{m_q} + C_{m_{\dot\alpha}}$ damping-in-pitch parameter, per radian

$C_{m_\alpha} - \left(\frac{\omega d}{V}\right)^2 C_{m_{\dot{q}}}$ oscillatory longitudinal stability parameter, per radian

A dot above a symbol indicates a first derivative with respect to time.

APPARATUS AND MODEL

The tests were made in the Langley 8-foot transonic pressure tunnel, which has a rectangular test section with longitudinal slots in the upper and lower walls. Tunnel stagnation temperature was automatically maintained at 122° F, and the humidity was held at a level such that the airstream was free of condensation shocks.

For the static tests, the sting-supported model was mounted on a three-component internal strain-gage balance, which measured normal force, axial force, and pitching moment. Model-balance chamber pressure and base pressure were measured at orifices located in the balance chamber and at the base annulus of the model. (See fig. 2.)

For the dynamic tests the model was mounted on a sting-supported single degree-of-freedom oscillating moment balance which was rigidly forced to perform an essentially sinusoidal angular pitching oscillation of 2° amplitude. Details of the dynamic stability measuring equipment are described in reference 2. Static pitching moments were also computed from measurements obtained with the dynamic balance locked at 0° amplitude.

Dimensions of the model, which was machined from aluminum, are presented in figure 2. For the dynamic tests, the model was equipped with two types of transition roughness. One form was a $\frac{1}{16}$-inch-wide circular band of sparsely distributed No. 80 carborundum grains on the model front face (fig. 2). The second type consisted of four concentric rings of approximately 18-mesh wire screen bonded to the model front face (figs. 2 and 3). For dynamic tests, the model was mounted on the balance with the oscillation axis coincident with the proposed center-of-gravity location (fig. 2). A photograph of the model installed in the wind tunnel is presented in figure 3.

TESTS

Both the dynamic and the static tests were made at Mach numbers of 0.60, 0.80, 1.00, and 1.20. Most tests were made at a tunnel stagnation pressure of one atmosphere with an associated range of Reynolds number (based on maximum body diameter) of 2.04×10^6 to 2.72×10^6. A few tests were also made at higher stagnation pressures for several Mach numbers as shown in tables I and II. Reynolds numbers attainable at these elevated stagnation pressures as well as the range for one atmosphere are indicated in figure 4.

All tests on the three-component static balance were made with aerodynamically smooth exposed surfaces through an angle-of-attack range of -3° to 18.3°. The axial-force data are presented as gross values and were not adjusted to a condition of free-stream static pressure at the base.

For the dynamic tests, the model was equipped with two types of transition roughness. Comparative static moment tests for both types of transition roughness were made with the dynamic balance in the locked position. Reduced frequency $\omega d/V$ for the dynamic tests varied from 0.018 to 0.058, and the amplitude of oscillation was 2°. Angle of attack for the dynamic tests was varied from 0° to 14°. With the exception of the high and low frequency data taken up to 18°, all wind-on dynamic data were taken at frequencies near the natural frequency of the oscillating model system for greater accuracy in the measurement of the damping moment (ref. 3).

ACCURACY

The ability of this forced-oscillation method to determine accurately the damping and oscillatory stability characteristics is discussed in references 2 and 3. For the present tests, repeat points checked very well except where the model flow conditions were critical, and the measured moments were highly dependent on the detailed flow over the model.

When a definite flow condition was well established, the probable error in the damping-in-pitch parameter $C_{m_q} + C_{m_{\dot{\alpha}}}$ is about ± 0.20 and in the oscillatory longitudinal stability parameter $C_{m_\alpha} - \left(\frac{\omega d}{V}\right)^2 C_{m_q}$ is about ± 0.02. Other accuracies are estimated to be within the following limits:

C_A	±0.018
C_N	±0.018
C_m	±0.005
M	±0.005
α	±0.20

RESULTS AND DISCUSSION

The static longitudinal stability parameters are presented in figure 5 for the test conditions shown in table I. The dynamic longitudinal stability parameters $C_{m_q} + C_{m_{\dot{\alpha}}}$ and $C_{m_\alpha} - \left(\frac{\omega d}{V}\right)^2 C_{m_{\dot{q}}}$ are presented in figures 6 to 8 for the test conditions shown in table II.

A comparison plot of the static pitching-moment coefficient slopes C_{m_α} and the oscillatory longitudinal stability parameter $C_{m_\alpha} - \left(\frac{\omega d}{V}\right)^2 C_{m_{\dot{q}}}$ for the various test conditions is presented in figure 9. Static C_{m_α} may be thought of as the oscillatory stability parameter at a reduced frequence $\omega d/V$ of 0.

Generally a negative value of the static stability parameter C_{m_α} (indicating a stable condition) was obtained for most test conditions; however, slight neutral stability appeared near $\alpha = 4^\circ$ for certain test conditions (figs. 5(a) and 9). Increased Reynolds number (flagged symbols) had negligible effects on the static pitching-moment coefficient but caused some changes in normal-force coefficient at angles of attack above about 6° for Mach numbers of 0.60 and 0.80 (figs. 5(a) and 5(b)). At subsonic speeds, front face surface condition had large effects on the static pitching moment especially at $M = 0.60$. Although a detailed description of the flow phenomena associated with the changes in surface condition and Reynolds number at $M = 0.60$ is not possible without measurements of the pressure distributions, a plausible explanation of the effects consistent with the observed results as well as with results obtained in other investigations (for example, refs. 4, 5, and 6), may be helpful. Application of carborundum roughness, selected on the basis of reference 7, fixed the boundary-layer transition on the front face and permitted a greater degree of flow expansion around the windward portion of the body shoulder at positive angles of attack. The decrease in the local pressures in the vicinity of the windward shoulder resulted in the more negative pitching moments measured. The wire-mesh roughness, which was much larger in magnitude than the carborundum, not only fixed transition but most likely caused an additionally large increase in the

thickness of the turbulent boundary layer, which was then more susceptible to separation over the windward shoulder region; fixing transition resulted in a decrease in the negative pressure and in the pitching-moment increment. As would be expected, at the higher Mach numbers, where greater flow expansion is possible even with a laminar boundary layer, the effect of surface condition decreases. For the smooth model, an increase in Reynolds number of less than a factor of 2 had little effect on the pitching moments although the negative increments in normal-force coefficient shown in figure 5(b) indicate some increase in flow expansion and in resultant negative pressures over the windward surfaces.

The damping-in-pitch parameter $C_{m_q} + C_{m_{\dot{\alpha}}}$ was very erratic, varying between values of approximately 3 and -2, and was dependent upon Mach number, angle of attack, reduced frequency (fig. 6), model surface condition (fig. 7), and Reynolds number (fig. 8). Note that Reynolds number is a function of stagnation pressure. (See fig. 4.) This dependency of the damping parameter on the detailed flow conditions over the body is typical of bluff, low-fineness-ratio bodies of revolution of this type as pointed out in reference 8. The changes in flow conditions also caused detailed changes in the oscillatory stability parameter $C_{m_\alpha} - \left(\frac{\omega d}{V}\right)^2 C_{m_{\dot{q}}}$ but did not appreciably affect the level of stability (figs. 6, 7, and 8). This parameter was relatively insensitive to changes in reduced frequency. Increases (or decreases) in the stability parameter with angle of attack generally were accompanied by decreases (or increases) in the damping parameter, a trend also described in references 8, 9, and 10.

Figure 9 shows the good agreement between the static and oscillatory stability data and indicates only minor effects of frequency.

CONCLUDING REMARKS

The results of tests made in the Langley 8-foot transonic pressure tunnel on a model of a low-fineness-ratio, blunted, cylindrical reentry body having a converging truncated-cone afterbody indicate that in general the body had static longitudinal stability throughout the range of test conditions, with small areas of neutral stability. The damping-in-pitch parameter varied erratically from values of approximately 3 to -2 and was affected by Mach number, angle of attack, reduced frequency, surface condition, and Reynolds number. The oscillatory longitudinal stability parameter showed good agreement with the static pitching-moment coefficients and in general showed stability throughout with small areas of neutral stability near $\alpha = 4^\circ$ and except for being relatively

insensitive to reduced frequency was also dependent on the aforementioned factors. The results emphasize the strong influence that streamflow and configuration-surface condition can have on the aerodynamic characteristics of bodies of this type.

Langley Research Center,
National Aeronautics and Space Administration,
Langley Air Force Base, Va., January 22, 1962.

REFERENCES

1. Lichtenstein, Jacob H.: Analytical Investigation of the Dynamic Behavior of a Nonlifting Manned Reentry Vehicle. NASA TN D-416, 1960.

2. Bielat, Ralph P., and Wiley, Harleth G.: Dynamic Longitudinal and Directional Stability Derivatives for a 45° Sweptback-Wing Airplane Model at Transonic Speeds. NASA TM X-39, 1959.

3. Braslow, Albert L., Wiley, Harleth G., and Lee, Cullen Q.: Dynamic Directional Stability Derivatives for a 45° Swept-Wing—Vertical-Tail Airplane Model at Transonic Speeds and Angles of Attack, With a Description of the Mechanism and Instrumentation Employed. NASA RM L58A28, 1958.

4. Fisher, Lewis R., Keith, Arvid L., Jr., and DiCamillo, Joseph R.: Aerodynamic Characteristics of Some Families of Blunt Bodies at Transonic Speeds. NASA MEMO 10-28-58L, 1958.

5. Polhamus, Edward C.: Effect of Flow Incidence and Reynolds Number on Low-Speed Aerodynamic Characteristics of Several Noncircular Cylinders With Applications to Directional Stability and Spinning. NASA TR R-29, 1959.

6. Polhamus, Edward C., Geller, Edward W., and Grunwald, Kalman J.: Pressure and Force Characteristics of Noncircular Cylinders as Affected by Reynolds Number With a Method Included for Determining the Potential Flow About Arbitrary Shapes. NASA TR R-46, 1959.

7. Braslow, Albert L., and Knox, Eugene C.: Simplified Method for Determination of Critical Height of Distributed Roughness Particles for Boundary-Layer Transition at Mach Numbers From 0 to 5. NACA TN 4363, 1958.

8. Wiley, Harleth G., Kilgore, Robert A., and Hillje, Ernest R.: Dynamic Directional Statility Characteristics for a Group of Blunt Reentry Bodies at Transonic Speeds. NASA TM X-337, 1960.

9. Igoe, William B., and Hillje, Ernest R.: Transonic Dynamic Stability Characteristics of Several Models of Project Mercury Capsule Configurations. NASA TM X-554, 1961.

10. Kilgore, Robert A., and Hayes, William C., Jr.: Transonic Wind-Tunnel Measurements of the Damping in Pitch and Oscillatory Longitudinal Stability of Several Reentry Vehicles Having Low Lift-Drag Ratios. NASA TM X-609, 1961.

TABLE I.- TEST CONDITIONS FOR STATIC LONGITUDINAL STABILITY DATA

[See fig. 4 for Reynolds numbers corresponding to different stagnation pressures]

Figure	Data presented	Surface condition	M	Tunnel stagnation pressure, atm	α, deg
5(a)	C_m	Smooth	0.60 to 1.20	1.0	-3 to 18.3
		Smooth	.60	1.7	-3 to 18.2
		Smooth	.80	1.6	-3 to 18.2
		Carborundum	.60 to 1.20	1.0	0 to 14
		Wire mesh	.60 to 1.20	1.0	0 to 14
5(b)	C_N	Smooth	0.60 to 1.20	1.0	-3 to 18.3
			.60	1.7	-3 to 18.3
			.80	1.6	-3 to 18.3
5(c)	C_A	Smooth	0.60 to 1.20	1.0	-3 to 18.3
			.60	1.7	-3 to 18.3
			.80	1.6	-3 to 18.3
5(d)	$C_{p,b}$ and $C_{p,c}$	Smooth	0.60 to 1.20	1.0	-3 to 18.3
			.60	1.7	-3 to 18.3
			.80	1.6	-3 to 18.3

TABLE II.- TEST CONDITIONS FOR THE DYNAMIC LONGITUDINAL STABILITY DATA

[See fig. 4 for Reynolds numbers corresponding to different stagnation pressures]

Figure	Surface condition	M	Tunnel stagnation pressure, atm	α, deg	$\frac{\omega d}{V}$
6	Carborundum	0.60 to 1.20	1.0	0 to 14	0.018 to 0.058
7	Wire mesh	0.60 to 1.20	1.0	0 to 14	0.023 to 0.046
	Carborundum	.60 to 1.20	1.0	0 to 14	.020 to .046
8	Carborundum	0.60 to 1.00	1.0	0 to 14	0.020 to 0.046
	Carborundum	.60 to .80	1.5	0 to 9	.033 to .044
	Carborundum	1.00 -	1.5	0 to 14	.024 to .036

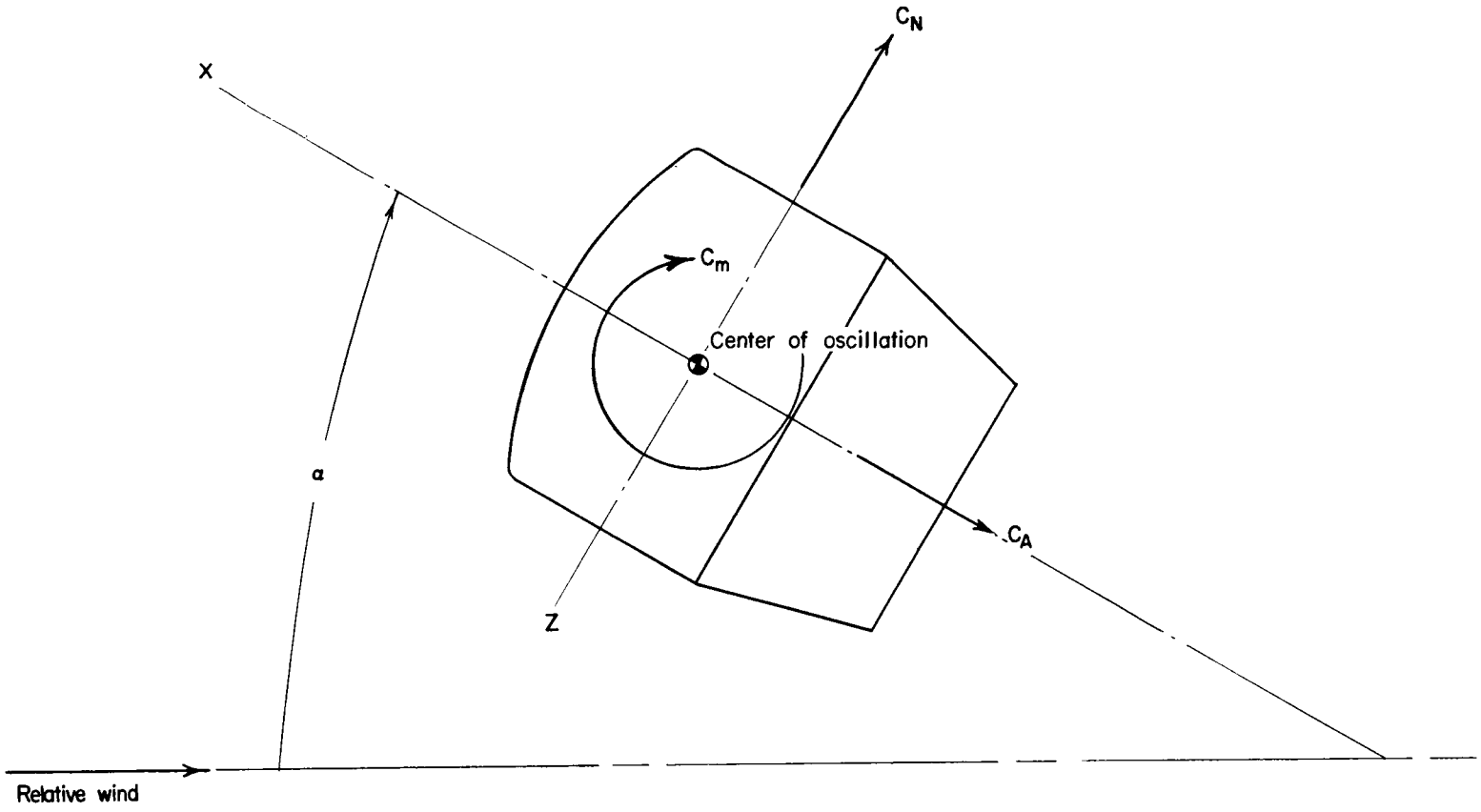

Figure 1.- Body-axis system. Arrows indicate positive directions of forces, moments, and angles.

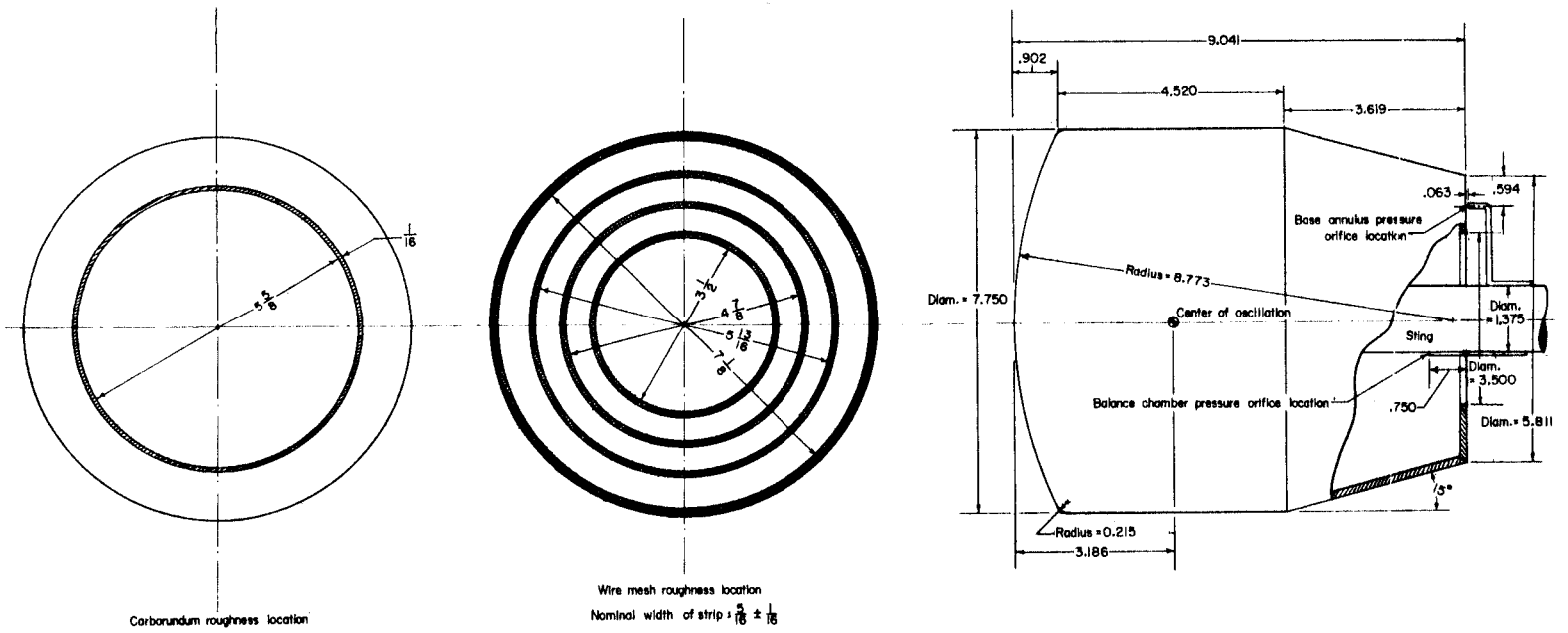

Figure 2.- Sketch of model tested. All dimensions are in inches unless otherwise noted.

L-60-8687

Figure 3.- Photograph of model with wire-mesh roughness.

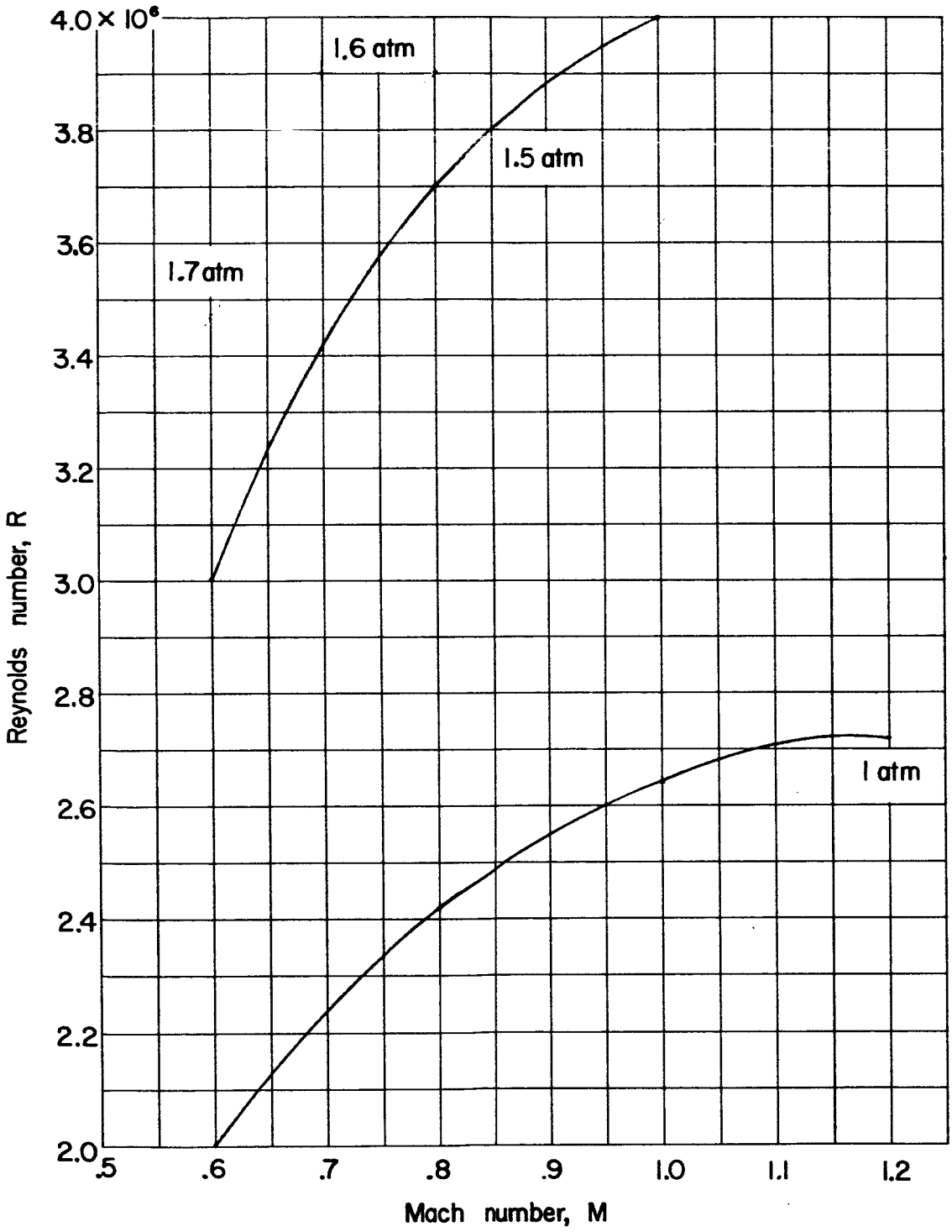

Figure 4.- Variation of Reynolds number with Mach number.

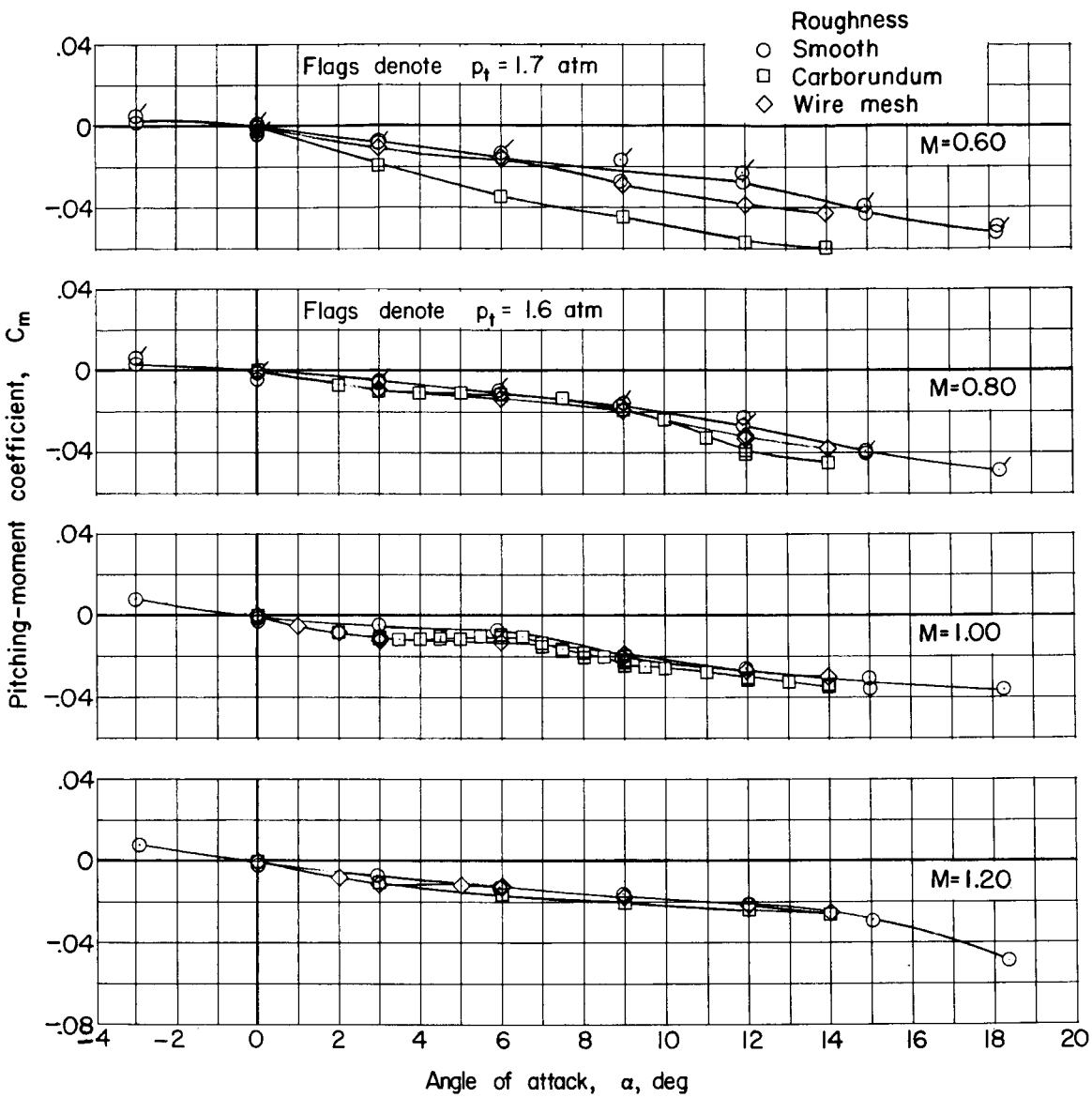

(a) Pitching-moment coefficient.

Figure 5.- Static longitudinal stability characteristics. Unflagged symbols are for p_t = 1.0 atm.

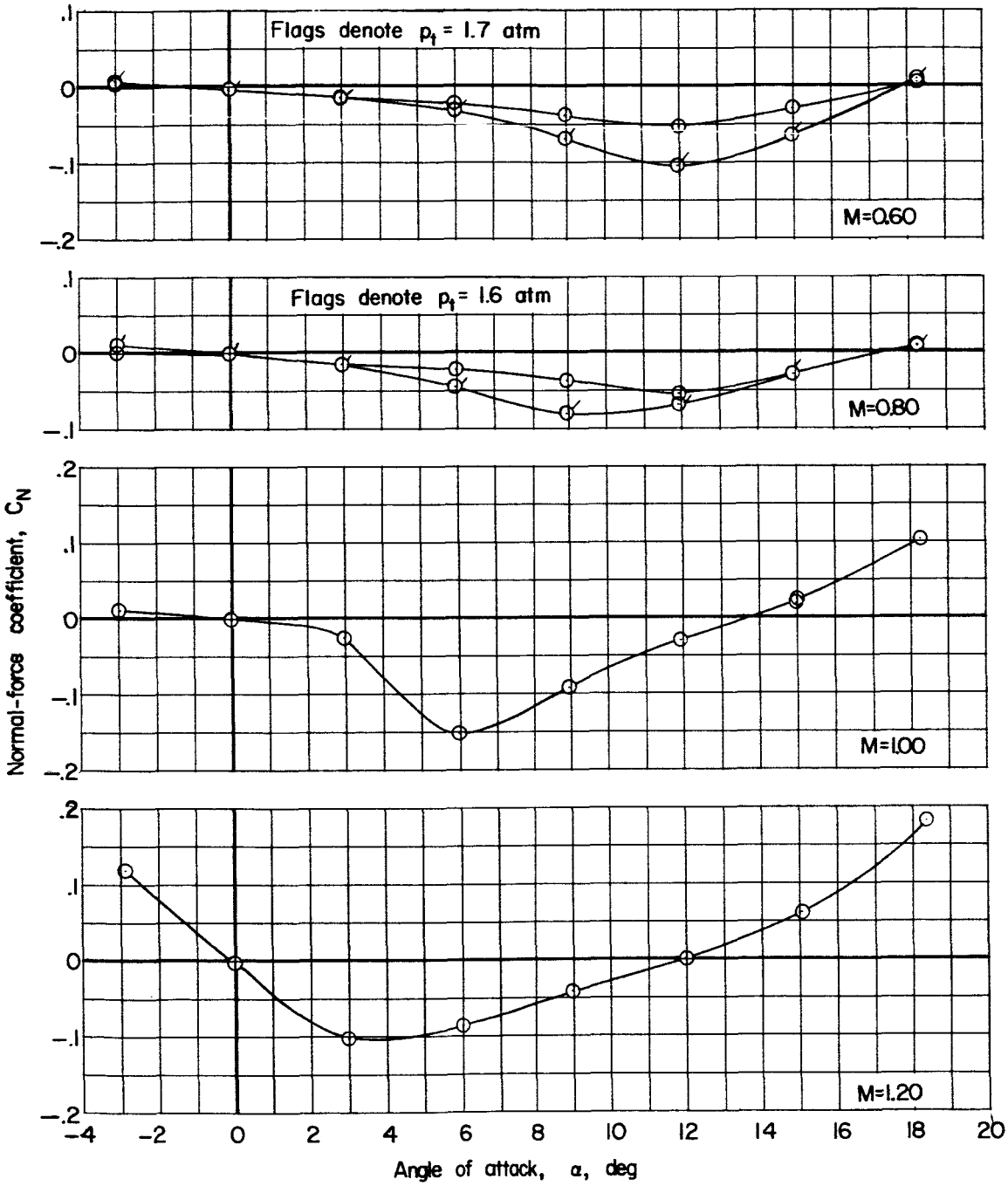

(b) Normal-force coefficient.

Figure 5.- Continued.

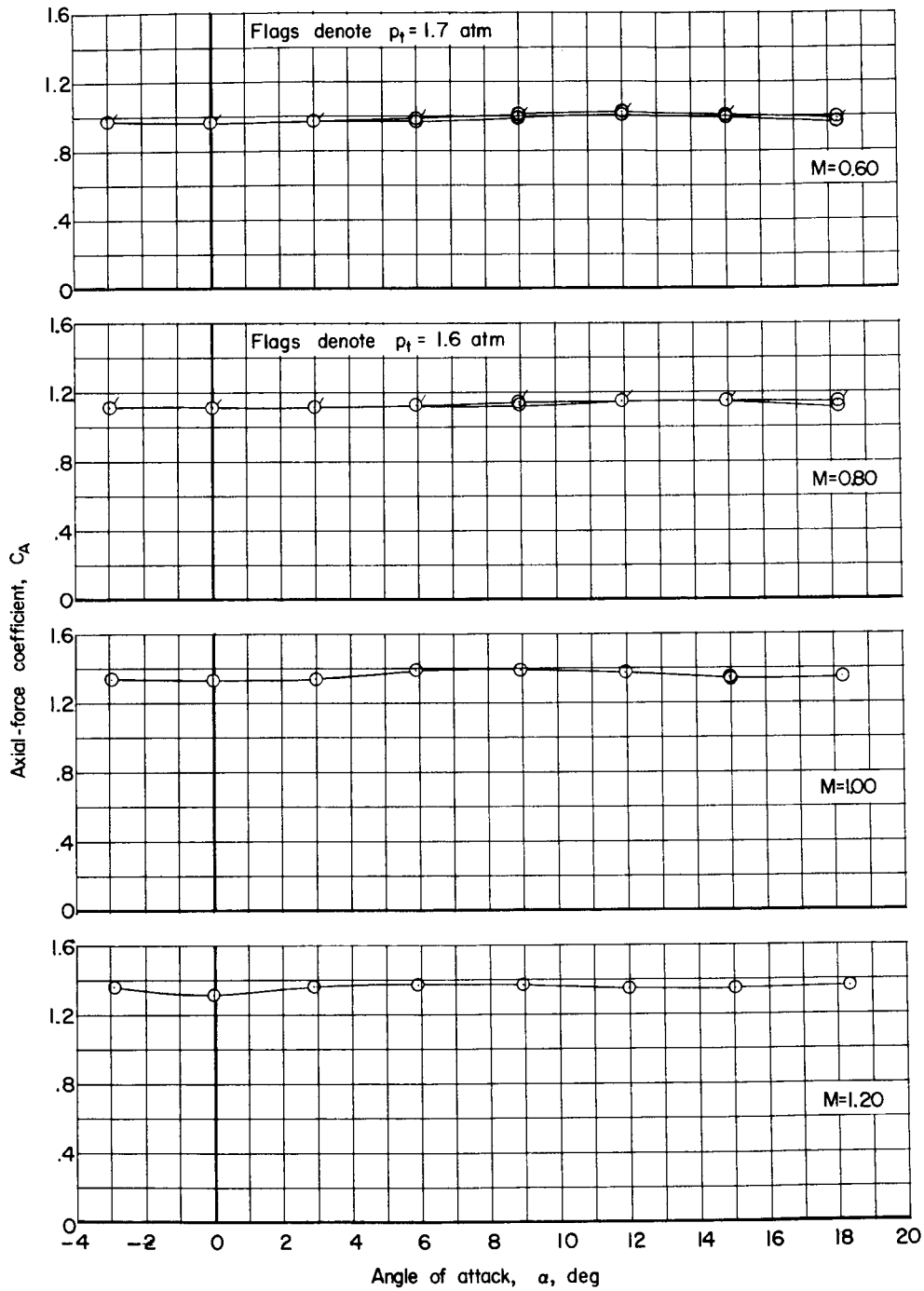

(c) Axial-force coefficient.

Figure 5.- Continued.

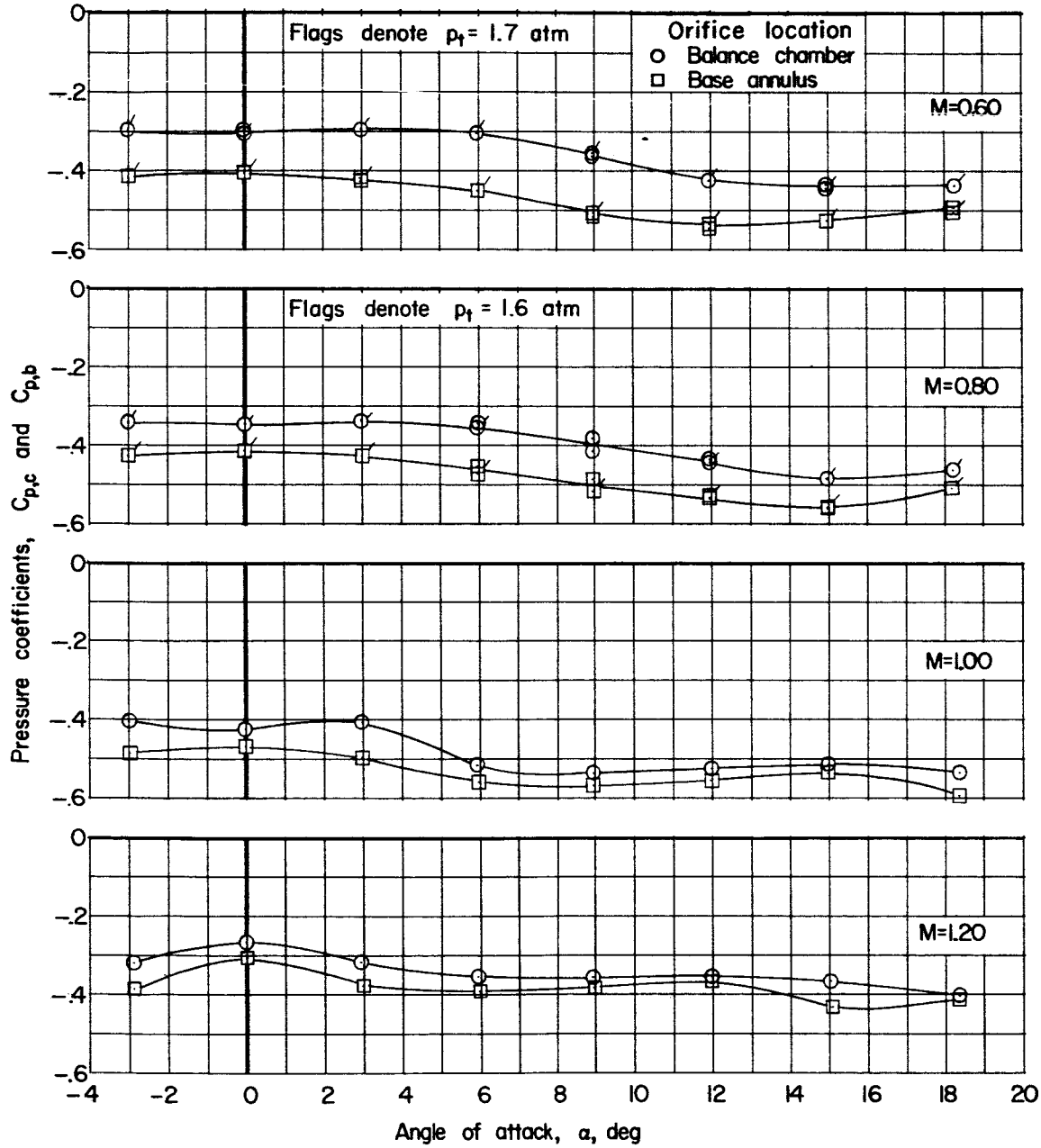

(d) Balance-chamber and base-pressure coefficients.

Figure 5.- Concluded.

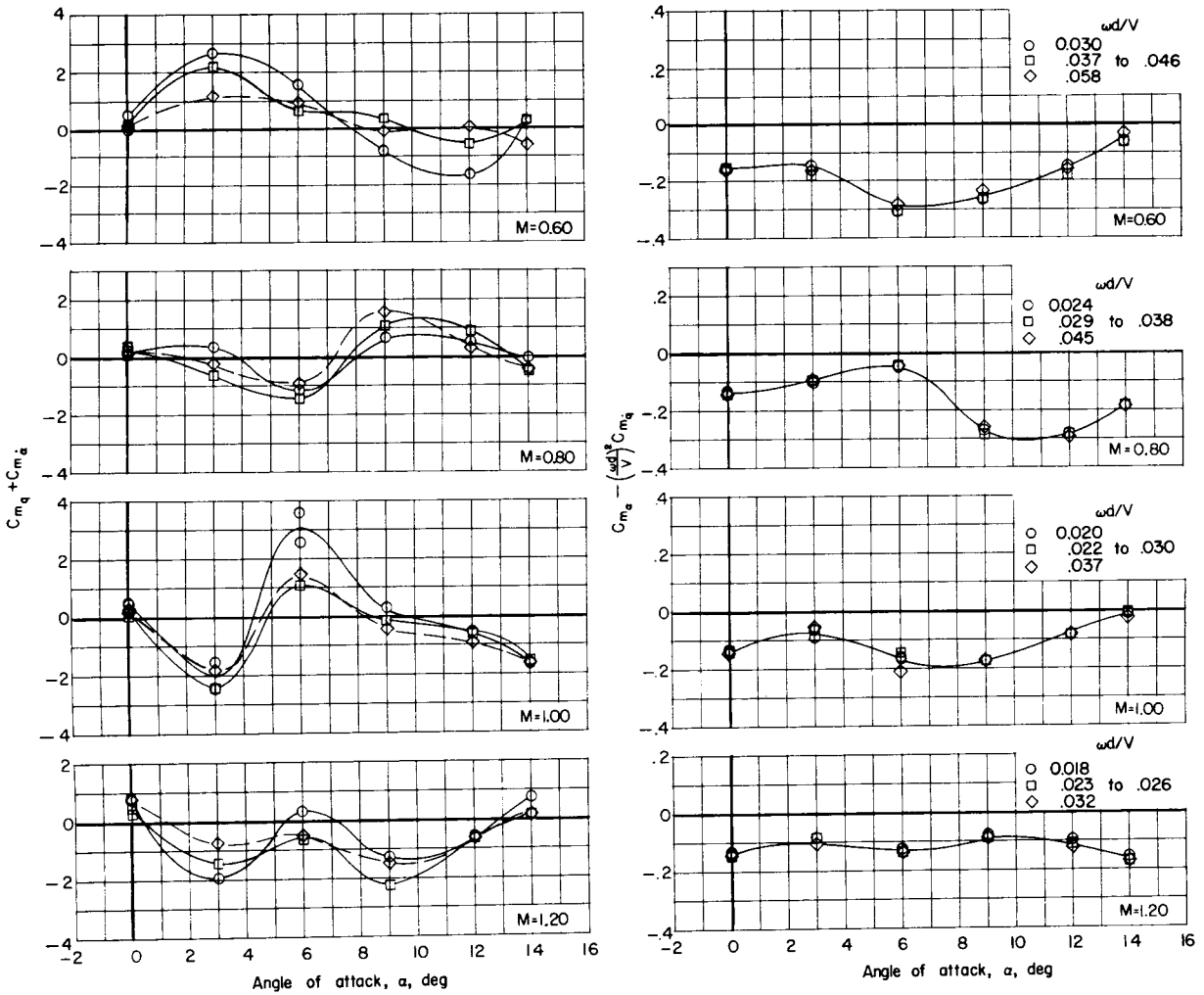

Figure 6.- Variation of the damping-in-pitch parameter and oscillatory longitudinal stability parameter with angle of attack for various Mach numbers and reduced frequencies. Stagnation pressure of 1.0 atmosphere. Carborundum roughness.

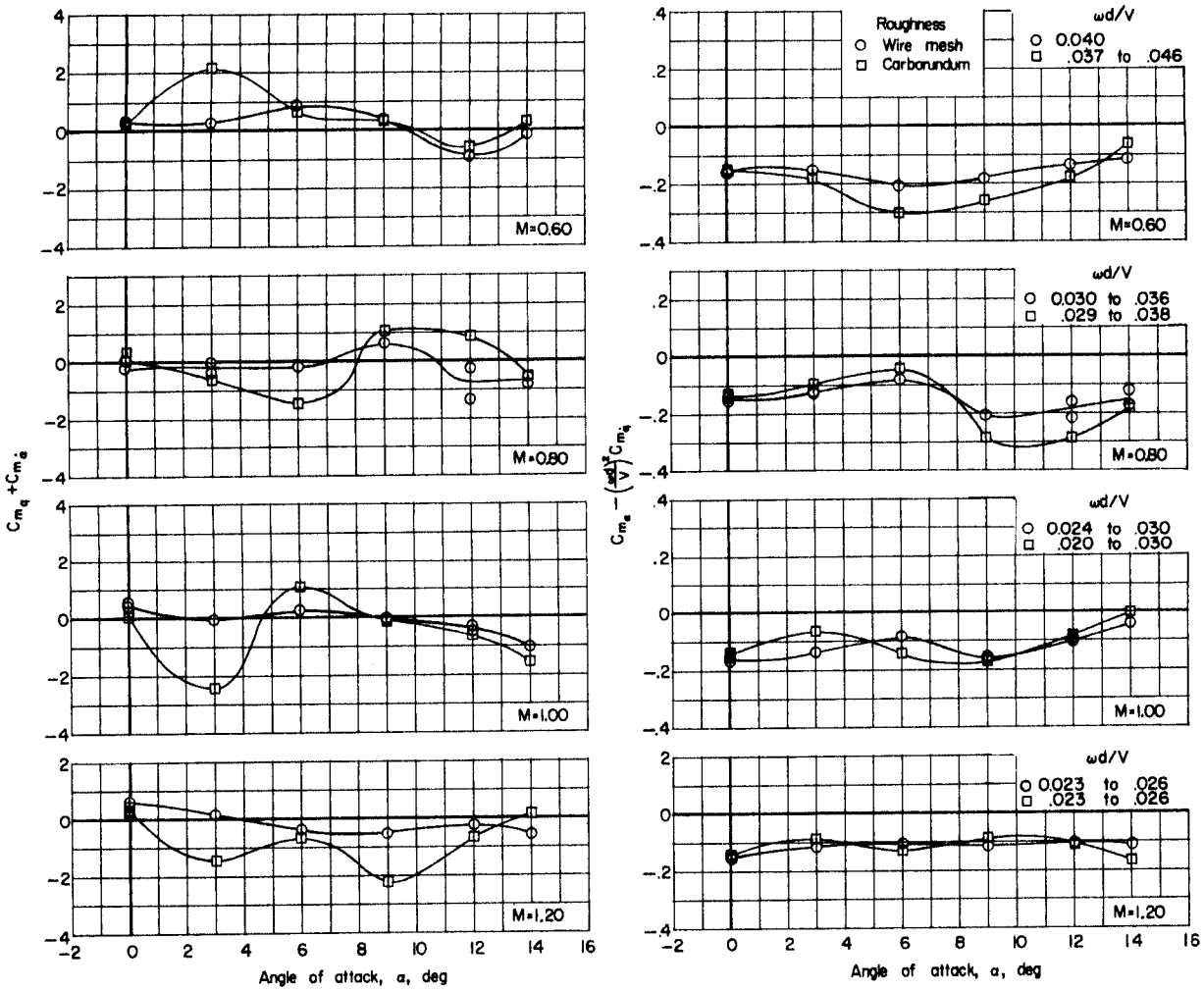

Figure 7.- Comparison of damping-in-pitch parameter and oscillatory longitudinal stability parameter for model with wire mesh and carborundum roughness. Stagnation pressure of 1.0 atmosphere.

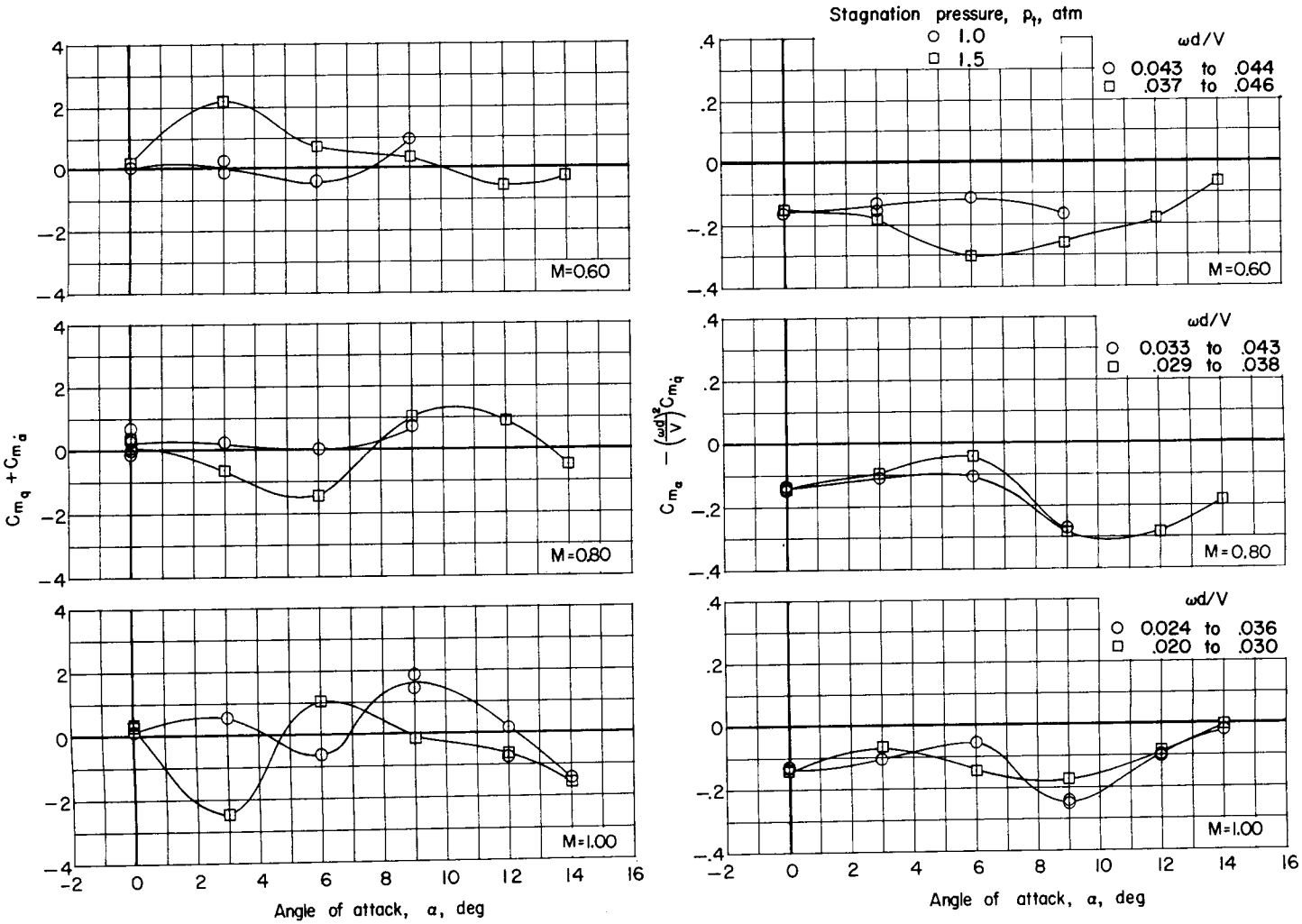

Figure 8.- Comparison of damping-in-pitch parameter and oscillatory longitudinal stability parameter for tests at stagnation pressures of 1.0 and 1.5 atmospheres. Carborundum roughness.

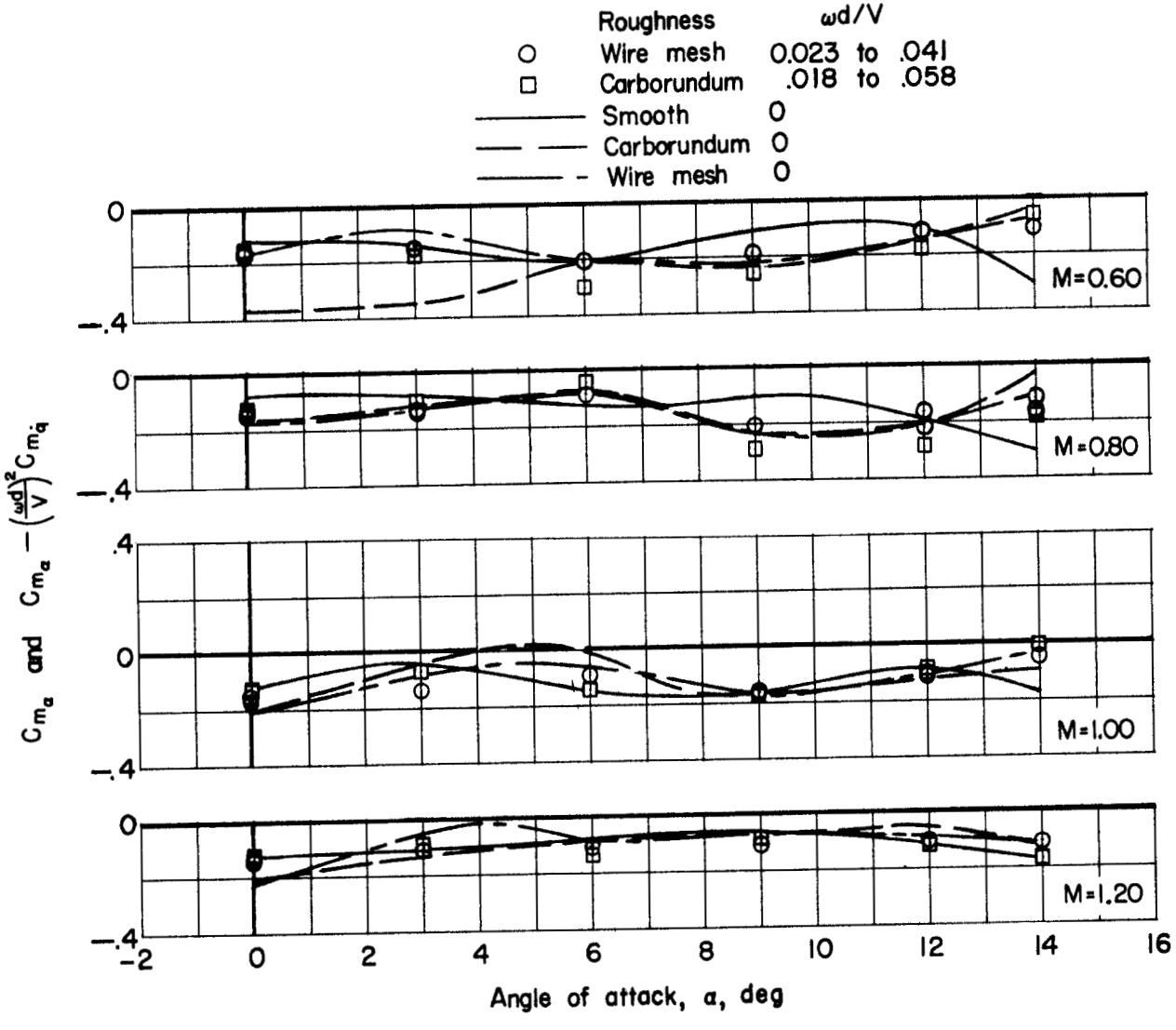

Figure 9.- Comparison of static and oscillatory longitudinal stability parameters.